COMSOL CONFERENCE 2024 FLORENCE

Ladle Furnace Preheating and Charge Heating with Graphite Heating Rods

Sergey Semenov[1], Patrick Namy[1], Aditya Kale[2], Sello Tsebe[2]
1. SIMTEC, Grenoble, France.
2. MINTEK, Randburg, South Africa.

Abstract
Present work is done in the framework of the SisAl Pilot EU project, which aims at optimising the silicon production in Europe by recycling materials and using a carbon-emission friendly technology. The silicon production experiments are conducted on laboratory and pilot scales in different types of furnaces, including ladle furnaces used as chemical reactors for molten slag-metal mixtures. Besides experimental work, the process optimisation also relies on the numerical modelling. In this work COMSOL Multiphysics® is used for the numerical testing of new thermal and electrical designs of a ladle furnace by simulating its preheating and charge heating in it with three graphite heating rods powered by a three-phase alternating current transformer. The one-heating-rod design was also tested. The following COMSOL® modules are employed: Heat Transfer in Solids and Fluids with phase change and convectively enhanced conductivity while fluid flow is not directly simulated, Surface-to-Surface Radiation, and Electric Currents to simulate the Joule effect in electrically conducting materials. A bidirectional coupling of all the modules is present due to multiple interdependencies via material properties. The model predicts that available electrical equipment is sufficient for preheating the empty ladle furnace up to 1600°C in less than 4 hours. Thanks to the model, the geometry of the heating rod was optimised to keep its temperature below 2500°C. It is found, however, that a modification of the electrical equipment would be needed to be able to heat the furnace charge with the heating rods submerged into it. The presented modelling approach for testing new furnace designs can be applied to other similar thermoelectrical problems.

Keywords: Ladle Furnace Preheating, Charge Heating, Graphite Heating Rods.

1. Introduction
This work is done in the framework of the SisAl Pilot EU project, which is focussed on demonstrating the possibility of metallurgical grade silicon production at pilot scale based on aluminothermic reduction of silica. In comparison with the traditional carbothermic reduction of silica, the advantage of the proposed technology is in its low CO2 emission. As part of the project, the numerical modelling support of experimental works is stipulated. One of the efforts is focussed on developing a numerical model of a new ladle furnace design proposed by MINTEK as a metallurgical reactor for the aluminothermic reaction between metal and slag. The objective of the present modelling work is to test thermal and electrical performance of the new furnace design during furnace preheating and aluminothermic reduction. The following hypotheses need to be tested: 1) the possibility of preheating ladle furnace up to 1600°C in less than 4 hours by using an existing MINTEK's electrical equipment, while keeping the temperature of graphite heating rods below 2500°C; 2) the possibility of continuous charge heating with help of three graphite heating rods submerged into the melt; 3) the risk of slag solidification during the aluminothermic reduction in the absence of external heating. In sections 2 and 3, model geometry and numerical methods are described. Sections 4 and 5 present governing equation and material properties. In section 6, numerical results are presented and discussed. Section 7 concludes the work.

2. Problem geometry
The ladle furnace, see Figure 1, has a cylindrical shape with a 120° sector symmetry. It consists of a graphite crucible containing furnace charge and gas, of three graphite heating rods placed symmetrically around the axis of rotation, refractory layers, and the steel shell separated from refractory by a calcium silicate board and a ceramic fibre blanket.

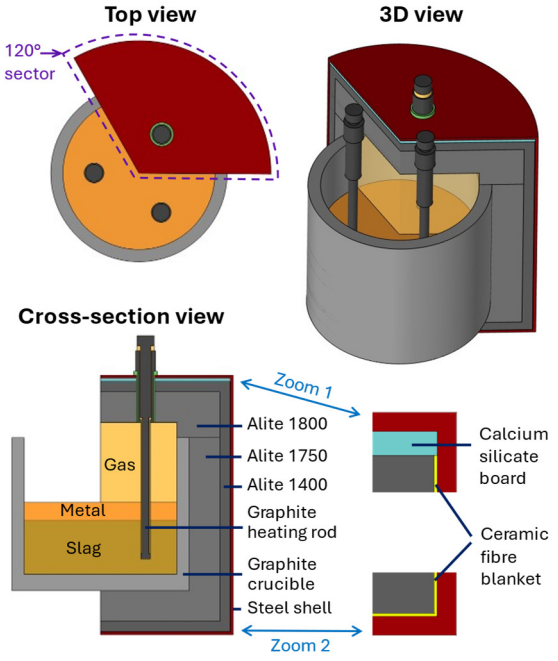

Figure 1. Modelled ladle furnace geometry and materials.

The thermal part of the problem benefits from the 120° sector symmetry, and therefore is resolved within only one 120° sector, see Figure 1. The electrical part of the problem, however, has no sector symmetry due to an electrical contact between three electrical phases via the electrically conducting furnace charge. Consequently, a complete 3D geometry is modelled for the electrically conducting parts of the furnace, including the furnace charge, the crucible, and the three heating rods. The heating rod geometry, see Figure 2, is based on an existing equipment at Elkem, one of the project partners, and is given three adjustable parameters a, b and c to have some degrees of freedom for the problem optimisation.

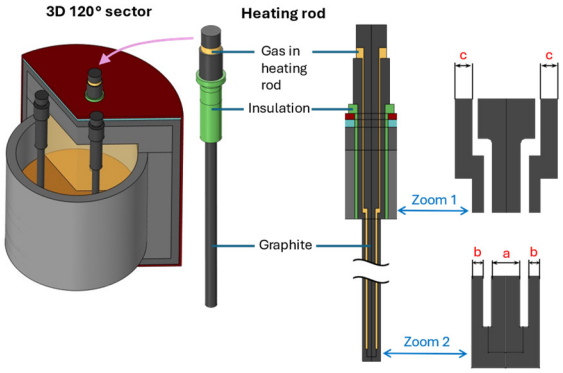

Figure 2. Heating rod geometry and materials.

3. Numerical methods

The problem is numerically solved with the finite element software COMSOL Multiphysics® version 6.0. The following modules have been used to setup the model physics: Heat Transfer in Solids and Fluids with phase change and convectively enhanced conductivity while fluid flow is not directly simulated, Surface-to-Surface Radiation, and Electric Currents to simulate the Joule effect in electrically conducting materials. A bidirectional coupling of all the modules is present due to multiple interdependencies via material properties.

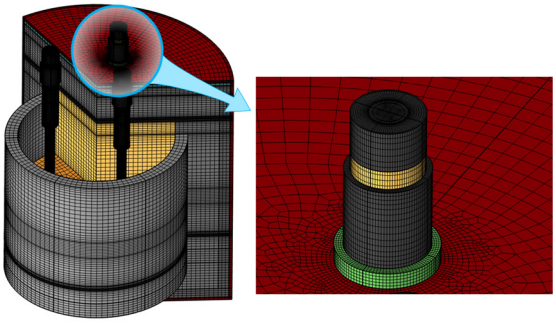

Figure 3. Spatial discretization mesh.

Each field was spatially discretized with linear Lagrange elements. Time integration is performed with the Backward Differentiation Formula (BDF) of order 1 to 2. The computational domain is spatially discretized with a quadrilateral mesh that consists of 1 195 000 finite elements, see Figure 3, resulting in 2 570 000 degrees of freedom. The computations are performed on 2 laptops with 8 physical cores Intel processor, 64 GB RAM, and a workstation with 64 physical cores and 1 TB RAM.

4. Governing Equations

4.1. Electric current equation

One of the requirements imposed by the ladle furnace design is the use of a 3-phase alternating current (AC) power source, such as one of the electrical transformers available at MINTEK. Thus, the present model implements the AC electrical equations in the frequency domain formulation. The equations of current conservation are solved in all electrically conducting domains (metal, slag, crucible and three heating rods):

$$\nabla \cdot \mathbf{j} = 0, \qquad \mathbf{j} = \sigma \mathbf{E} + j\omega \mathbf{D},$$
$$\mathbf{E} = -\nabla V, \qquad \mathbf{D} = \varepsilon_0 \varepsilon_r \mathbf{E}, \qquad \omega = 2\pi f$$

where $\mathbf{j}$ is the complex amplitude (or phasor) of the electric current density, $\mathbf{E}$ is the phasor of electric field, V is the phasor of electric potential, $\mathbf{D}$ is the phasor of electric displacement field, σ is the electrical conductivity as a function of temperature, f is the alternating current frequency, ω is the angular frequency, ε_0 is the vacuum permittivity, ε_r is the relative permittivity, and $j = \sqrt{-1}$ is the imaginary unit. The volume density of the heat source due to Joule effect is as follows:

$$Q = \frac{1}{2}\mathrm{Re}(\mathbf{j} \cdot \mathbf{E}^*)$$

where asterisk $\mathbf{E}^*$ denotes the complex conjugate of $\mathbf{E}$, and $\mathrm{Re}(Z)$ is the real part of the complex number Z. The electrical boundary conditions on the heating rod terminals, see Figure 4, are defined by the electrical transformer that powers up the furnace and by the type of 3-phase electrical connection of the heating rods: either delta (D) or star (Y) connection.

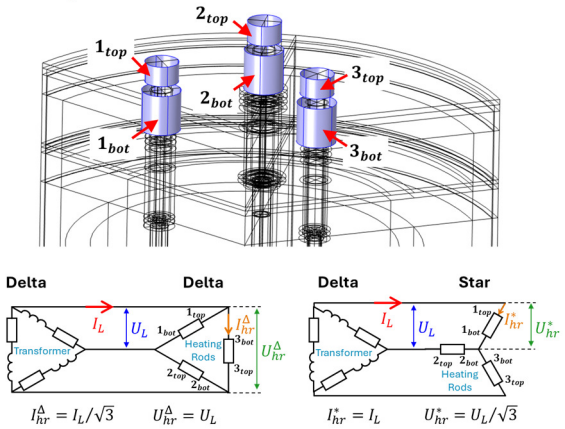

Figure 4. Heating rod terminals and connection types.

Here, U_L and I_L are the effective line voltage and the effective line current, U_{hr}^{Δ} and I_{hr}^{Δ} are the effective voltage and the effective current through a heating rod in the delta configuration, and U_{hr}^{*} and I_{hr}^{*} are those in the star configuration. Boundary conditions for the electric potential at the top terminals read:

$$V_{i_{top}} = \sqrt{2} U_{hr}^{*} e^{j\varphi_i} = \frac{\sqrt{2}}{\sqrt{3}} U_L e^{j\varphi_i}, \qquad i = 1, 2, 3$$

with line phases $\varphi_i = i \cdot 120°$. For the bottom terminals, in case of star connection:

$$V_{i_{bot}} = V^*_{i_{bot}} = 0, \qquad i = 1,2,3$$

and in case of delta connection:

$$V_{i_{bot}} = V^{\Delta}_{i_{bot}} = \frac{\sqrt{2}}{\sqrt{3}} U_L e^{j(\varphi_i + 120°)}, \qquad i = 1,2,3$$

Electric insulation is assumed on other external boundaries of the electrically conducting domain:

$$\mathbf{j} \cdot \mathbf{n} = 0$$

4.2. Heat transfer with surface-to-surface radiation

The following heat equation is solved in all domains of the 120° sector shown in Figure 1:

$$\rho c_p' \frac{\partial T}{\partial t} + \nabla \cdot \mathbf{q} = Q, \qquad \mathbf{q} = -\max(1, \mathrm{Nu}) \cdot k \nabla T$$

where T is temperature, t is time, ρ is density, $\mathbf{q}$ is the convectively enhanced conductive heat flux, k is the thermal conductivity, c_p' is the isobaric specific heat capacity modified with the Apparent Heat Capacity method to account for phase changes, Q is the volume density of heat source due to the Joule effect in electrically conducting materials and the heat loss in the crucible gas due to a protective gas flow with the modelled rate of $8\,\mathrm{L/min}$. The conductivity k is convectively enhanced in the crucible gas with the Nusselt number Nu, which is computed according to an empirical model as a function of temperature difference between the heating rod and the crucible. Zero normal heat flux is imposed at the two symmetry planes, see Figure 5:

$$\mathbf{q} \cdot \mathbf{n} = 0$$

where $\mathbf{n}$ is the unit normal vector to the symmetry plane.

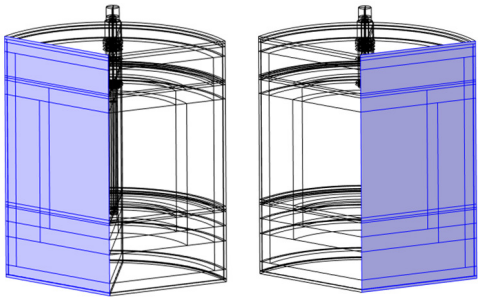

Figure 5. In blue: two symmetry planes.

As the electrical cables connected to heating rods are supposed to be water cooled, the ambient temperature T_{amb} is imposed on the heating rod terminals, see Figure 6 (a):

$$T = T_{amb}$$

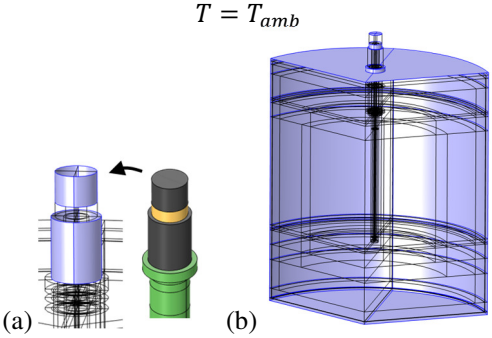

(a) (b)

Figure 6. In blue: (a) heating rod terminals, (b) other external boundaries of the furnace.

On other external surfaces of the furnace, see Figure 6 (b), the heat flux due to external natural convection is applied:

$$\mathbf{q} \cdot \mathbf{n} = h(T - T_{amb})$$

where $\mathbf{n}$ is the outward unit normal vector and h is the heat transfer coefficient computed according to several empirical models of external natural convection: one for a thin vertical cylinder and two models for the upside and downside horizontal plates. Temperature continuity on all material interfaces is applied:

$$T_{up} = T_{down}$$

where subscripts up and $down$ denote opposite sides of the interface with up corresponding to the positive direction of the normal vector $\mathbf{n}$. The condition of heat flux continuity/discontinuity at material interfaces writes:

$$\mathbf{q}_{up} \cdot \mathbf{n} - \mathbf{q}_{down} \cdot \mathbf{n} = q$$

where q is the surface density of the interfacial heat source in $\mathrm{W/m^2}$. In the presence of both metal and slag, an interfacial heat source q at the metal-slag interface due to aluminothermic reduction is computed based on the reaction energy and the reaction time. The interfaces adjacent to gases (in the crucible and in the heating rod) participate in the surface-to-surface radiation and thus have the following interfacial heat source q:

$$q = \varepsilon(G_{rad} - \sigma_{SB} T^4)$$

where ε is the hemispherical emissivity of radiating surfaces, σ_{SB} is the Stefan-Boltzmann constant, and G is the surface irradiance (surface density of the radiant flux, in $\mathrm{W/m^2}$, that arrives to the surface). A special 120° rotation symmetry condition is applied for the surface-to-surface radiation problem, which is not equivalent to a conventional zero-flux symmetry condition but allows radiant heat fluxes to pass through the symmetry planes.

5. Material properties and parameters

5.1. Graphite

For simplicity, the model of graphite uses its porosity ϕ, including both open and closed pores, as a single adjustable parameter of the material, which, alongside with temperature T, defines all other material properties. We also assume that porosity ϕ does not change with temperature T. The graphite density ρ_{gr} is modelled as a linear function of porosity ϕ:

$$\rho_{gr}(T, \phi) = (1 - \phi)\rho_C(T)$$

where $\rho_C(T)$ is the density of non-porous graphite, which is modelled as function of temperature by using the linearized thermal expansion coefficient:

$$\alpha_V(T) = -\frac{1}{\rho_C(T)} \left(\frac{\partial \rho_C(T)}{\partial T} \right)_p = \alpha_{V,\mathrm{ref}} + (\alpha_V)_T' \left(T - T_{\mathrm{ref},\alpha} \right)$$

and the theoretical density of non-porous graphite at a given temperature:

$$\rho_{C,\mathrm{ref}} = 2260\,\mathrm{kg/m^3} \quad \text{at} \quad T_{\mathrm{ref},\rho} = 293\,\mathrm{K}$$

Assuming constant pressure $p = const$ and integrating both sides of $\alpha_V(T)$ expression, we get:

$$\rho_C(T) = \rho_{C,\text{ref}} \exp\left(-\alpha_V(T)\theta + (\alpha_V)'_T \frac{\theta^2}{2}\right)$$

where $\theta = T - T_{\text{ref},\rho}$. Using the above theoretical density model $\rho_{gr}(T,\phi)$ and fitting the value, the slope and the second derivative of the temperature-dependent graphite density found in literature [1], see Figure 7, we obtain the theoretical porosity ϕ of given material samples, see Figure 7, as well as the following thermal expansion constants:

$$\alpha_{V,\text{ref}} = 1.4508 \times 10^{-5}\ \text{K}^{-1} \quad \text{at} \quad T_{\text{ref},\alpha} = 293\ \text{K}$$
$$(\alpha_V)'_T = 6.9518 \times 10^{-9}\ \text{K}^{-2}$$

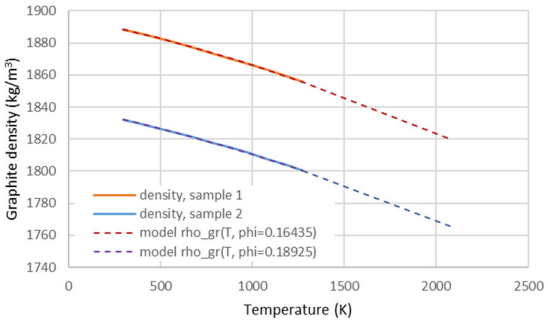

Figure 7. Fitting graphite density from literature [1] (samples 1 and 2) with the theoretical density model.

The graphite's specific heat capacity at constant pressure $c_{p,gr}(T)$ is assumed to be independent of the material porosity:

$$c_{p,gr}(T) = \begin{cases} c_{p,\text{cub}}(T), & T \le T_1 = 300\ \text{K} \\ c_{p,\text{app}}(T), & T > T_1 = 300\ \text{K} \end{cases}$$

where $c_{p,\text{app}}$ approximates literature data:

$$c_{p,\text{app}}(T) = -5.8068 \times 10^{-17} \cdot \text{T}^6 + 6.8603 \times 10^{-13} \cdot T^5 - 3.2774 \times 10^{-9} \cdot T^4 + 8.1193 \times 10^{-6} \cdot T^3 - 1.1138 \times 10^{-2} \cdot T^2 + 8.4443 \cdot T - 1.0091 \times 10^3$$

and $c_{p,\text{cub}}$ is the cubic continuation of $c_{p,\text{app}}$:

$$c_{p,\text{cub}}(T) = \left.\frac{dc_{p,\text{app}}(T)}{dT}\right|_{T=T_1} (T - T_1)\frac{T^2}{T_1^2} + c_{p,\text{app}}(T_1)\left(3 - \frac{2T}{T_1}\right)\frac{T^2}{T_1^2}$$

where T is in K and $c_{p,\text{app}}$ and $c_{p,\text{cub}}$ are in J/kg/K. The thermal k_{gr} and the electrical conductivity σ_{gr} of graphite are modelled as functions of its porosity ϕ using the Landauer's model of conductivity of a porous medium based on the effective medium percolation theory [2]:

$$k_{gr}(T,\phi) = f_L(k_C(T), k_{air}(T), \phi)$$
$$\sigma_{gr}(T,\phi) = f_L(\sigma_C(T), 0, \phi)$$

where $k_C(T)$ and $\sigma_C(T)$ are respectively the thermal and the electrical conductivity of non-porous graphite, $k_{air}(T)$ is the thermal conductivity of air trapped inside of pores, and f_L is given by [2]:

$$f_L(k_s, k_p, \phi) = \frac{1}{4}\left(s + \sqrt{s^2 - 8k_s k_p}\right)$$
$$s = k_p(3\phi - 1) + k_s(2 - 3\phi)$$

where k_s and k_p are respectively the solid and the pores conductivity. The temperature dependencies of non-porous graphite conductivities $k_C(T)$ and $\sigma_C(T)$ are obtained by fitting the graphite conductivities found in literature [1, 3] with the above presented theoretical models $k_{gr}(T,\phi)$ and $\sigma_{gr}(T,\phi)$, where porosity ϕ is already known from density fitting. Several curves of $k_C(T)$ and $\sigma_C(T)$ obtained in this way are then averaged, resulting in the following dependencies:

$$k_C(T) = 46758\ \text{W/(m} \cdot \text{K)} \cdot (T/1\text{K} + 405)^{-0.8543}$$
$$\sigma_C(T) = -7.1142 \times 10^{-15} \cdot T^6 + 6.5797 \times 10^{-11} \cdot T^5 - 2.50415 \times 10^{-7} \cdot T^4 + 5.2414 \times 10^{-4} \cdot T^3 - 0.67881 \cdot T^2 + 509.18 \cdot T + 6743.35$$

where T is in K and σ_C is in S/m. In the working range of furnace temperatures, the hemispherical emissivity of graphite ε_C varies between 0.5 and 0.85 [3]. The value of $\varepsilon_C = 0.5$ is used in the current model as it corresponds to the worst-case scenario when heating rod overheats faster. If we'll be able to avoid the overheating for $\varepsilon_C = 0.5$, then we'll also avoid it for the larger values of ε_C. The relative permittivity of graphite $\varepsilon_{r,gr}$ is taken as the volume average of the one of non-porous graphite $\varepsilon_{r,C} = 15$ and the one of air $\varepsilon_{r,air} = 1$:

$$\varepsilon_{r,gr} = (1 - \phi)\varepsilon_{r,C} + \phi\varepsilon_{r,air}$$

Thus, two types of graphite, the one for the crucible and the one for the heating rod, are assumed to be different only by their porosity. The porosity was calibrated by fitting experimental data for another furnace at Elkem that uses same graphite materials:

$$\phi_{\text{crucible}} = 0, \qquad \phi_{\text{heating rod}} = 0.08$$

5.2. Slag and metal

The metal phase, which is initially pure Al, becomes Al-Si-Ca alloy as it reacts with slag. Similarly, initially SiO_2-CaO slag becomes Al_2O_3-SiO_2-CaO slag as it reacts with metal. Thus, slag and metal densities are computed as functions of temperature T and composition X_i (mole fraction of component i):

$$\rho(T, X_i) = \sum_i [X_i M_i] / \left(\sum_i \left[X_i V_{m,i}(T)\right] + V^{EX}\right)$$

where M_i and $V_{m,i}$ are respectively the molar mass and the molar volume [4, 5, 6, 7] of component i, V^{EX} is a corrective interaction term [7], $i = \text{Al, Si, Ca}$ for metal and $i = \text{Al}_2\text{O}_3, \text{SiO}_2, \text{CaO}$ for slag. The composition of slag and metal is modelled as function of the relative reaction extent ξ_{rel} that equals 0 at the beginning of the process and 1 at the end of the reaction:

$$X_i = X_{i,init} + \xi_{rel}\left(X_{i,final} - X_{i,init}\right)$$

For simplicity, it is assumed that the relative reaction extent ξ_{rel} is a linear function of time:

$$\xi_{rel} = t/t_r$$

where t_r is the user defined reaction time. The initial $X_{i,init}$ and final $X_{i,final}$ compositions, as well as the reaction energy, are estimated with help of the software provided by the project partner SINTEF. This artificial-neural-network-based tool [8, 9] is trained on the FactSage® data for the metal-slag system of interest. Other metal properties, such as thermal and electrical conductivity [4], dynamic viscosity [10], and heat capacity at constant pressure

are computed as for pure aluminium. Slag thermal conductivity is assumed to be constant and equal to $1\,\mathrm{W/m/K}$. Other properties of the slag phase, such as heat capacity, enthalpy, viscosity and electrical conductivity are computed as functions of its temperature T and composition X_i according to the Ken Mills model [11].

5.3. Other materials

The heating rod gas is air, and the crucible gas is argon. Their density is computed according to the ideal gas law. Air heat capacity is taken from the COMSOL Multiphysics® materials library, whereas argon heat capacity is taken constant ($520\ \mathrm{J/kg/K}$). Thermal conductivity of both gases, as well as the viscosity of argon which is needed for the Nu number computation, are modelled according to the Sutherland's law [12]. The properties of the insulation material, see Figure 2, are experimentally unknown and therefore are arbitrarily selected: zero electrical conductivity, density $10^3\,\mathrm{kg/m^3}$, heat capacity $10^3\,\mathrm{J/kg/K}$, emissivity 0.85, and thermal conductivity $10\,\mathrm{W/m/K}$. The structural steel properties from the materials library are used for the steel shell. Its hemispherical emissivity is takes as for the iron oxide Fe_2O_3 [13]. The properties of refractory materials are taken from material data sheets provided by the refractory supplier: Elite Cast 1400 INS for the external layer of refractory, Elite ATB Cast 1750 for the internal body refractory, and Elite BA Cast 1800 INS for the internal roof refractory, see Figure 1. Calcium silicate board properties are taken from the technical data sheet for MB1000 Special material. Its thermal conductivity (in $\mathrm{W/m/K}$) is interpolated as function of T (in K):

$$k_{MB1000} = 9.7344 \times 10^{-9} \cdot T^2 + 2.5007 \times 10^{-6} \cdot T + 2.0106 \times 10^{-2}$$

Finally, properties of the ceramic fibre blanket are modelled according to the specifications of Fibermax® Matte for the density of $130\,\mathrm{kg/m^3}$. Its heat capacity is estimated based on its composition.

6. Numerical results and discussion

6.1. Furnace preheating and optimization of the heating rod geometry

Numerical simulations show that input power above 0.4 MW will be sufficient to preheat empty furnace crucible up to 1600°C in less than 4 hours, see Figure 8. However, even at 0.4 MW input power, dangerous temperatures above 2500°C are reached, Figure 9.

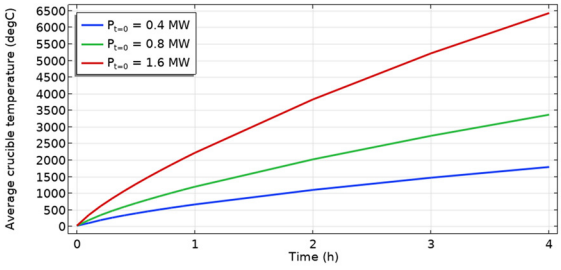

Figure 8. Computed average crucible temperature as function of time for different input power.

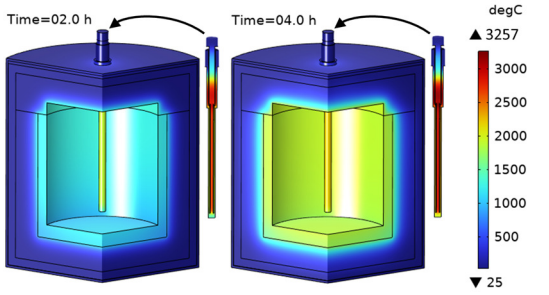

Figure 9. Temperature field for the input power of 0.4 MW.

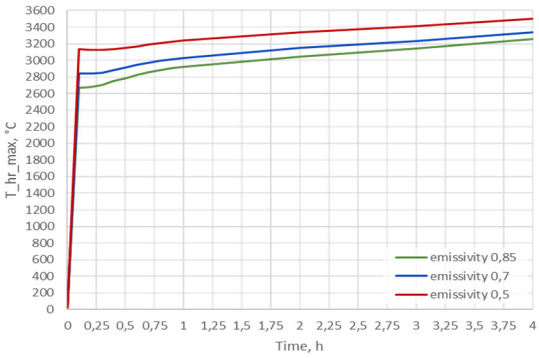

Figure 10. Maximum heating rod temperature at 0.4 MW input power for different graphite emissivity.

Increasing the heating rod emissivity decreases its maximum temperature $T_{hr,max}$, see Figure 10, but not enough to be below 2500°C. The natural gas convection in the crucible or the heat loss due to a protective gas flow through the crucible have almost negligeable influence on $T_{hr,max}$. Thus, the heating rod geometry was optimised by varying three parameters a, b, c (see Figure 2) to satisfy 3 criteria:

1) The historical maximum of the power dissipation in three heating rods should not exceed the maximum transformer power.
2) The average crucible temperature should reach 1600°C in less than 4 hours.
3) The maximum heating rod temperature $T_{hr,max}$ should not exceed 2500°C.

The result of such optimisation shows that delta (D) connection of heating rods, see Figure 4, should be avoided as it delivers too much power and overheats the rods even for the minimum available transformer voltage. Instead, the star (Y) connection of heating rods should be used. In this case, when the minimum line voltage of $U_L = 105\,V$ (as per available electrical equipment) is provided, the optimum geometry parameters are found to be:

$$a = 50\ \mathrm{mm},\quad b = 2\ \mathrm{mm},\quad c = 15\ \mathrm{mm}$$

With this heating rod geometry, the temperature field after 4 hours of furnace preheating is shown in Figure 11: maximum heating rod temperature is below 2408°C, while average crucible temperature is above 1600°C. The transformer delivers between 337 and 410 kW of heating power depending on the heating rod temperature at each moment in time. Note that in practice, besides the above three satisfied optimisation criteria, there is also a mechanical strength requirement: the minimum thickness of graphite parts must be greater than 1 cm.

As one can see, the thickness b does not satisfy this criterion and gets even thinner as line voltage increases. Nevertheless, the optimised geometry of rods will be used in further computations to study other thermal and electrical aspects of the furnace design.

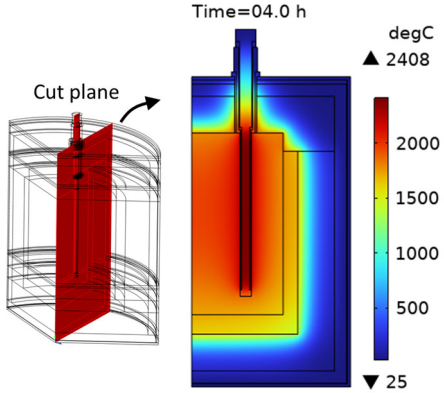

Figure 11. Temperature field after 4 hours of furnace preheating with an optimized geometry of heating rods. Line voltage is 105 V.

6.2. Charge heating with available transformer

Below we present the results of modelling of charge heating with submerged heating rods powered by the available transformer: $U_L = 105\,V$. The previously computed preheated state serves an initial condition. Initial slag temperature is 1650°C, initial metal temperature is 800°C. Two cases are investigated: **Case 1:** only slag is charged, **Case 2:** both slag and metal are charged. In **Case 1** there is no chemical reaction, and furnace is heated only by the electrical heat source. Figure 12 shows the computed temperature field before and after 30 min of heating.

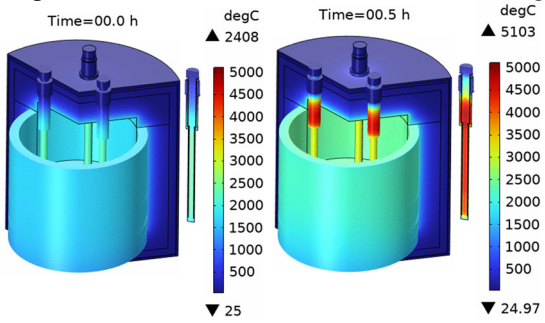

Figure 12. Temperature field when only slag is charged into the furnace. Line voltage is 105 V.

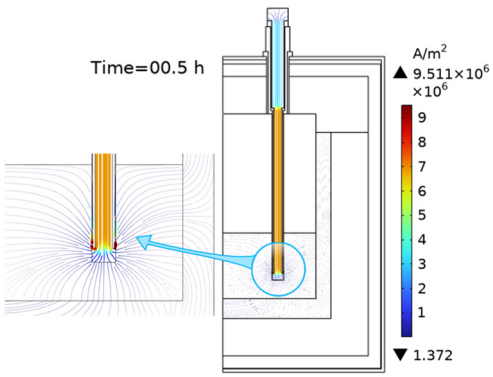

Figure 13. Map of the electric current density when only slag is charged into the furnace. Line voltage is 105 V.

As one can see, the temperature inside heating rods rises to 5103°C due to high electric currents passing through them, see Figure 13. The current goes down the internal graphite cylinder of the heating rod and then, instead of going up through the external graphite cylinder, it prefers to pass through the slag volume and the graphite crucible towards two other graphite rods also submerged into the slag. Apparently, this path is less resistive and creates a short-circuit between heating rods. The effective line current I_L approaches 10^4 A, which is 2 times above the allowed transformer's maximum and, therefore, is dangerous for the electrical equipment. Also, as the slag temperature rises due to heating provided, its electrical conductivity increases, which results in further growth of the electric current over time. To conclude **Case 1**, the presence of slag in the furnace results in a short-circuit between heating rods, in dangerous transformer currents, and in graphite overheating above 2500°C. Similar conclusion is made for the **Case 2**, when both slag and metal are charged. The heat produced by reaction and the high conductivity of metal do not improve the situation.

6.3. Charge heating with reduced line voltage

Let's consider the worst-case configuration when both slag and metal are charged into the furnace. In this case we can try to reduce the effective line voltage U_L so that it provides a reasonable electric power input and avoids the above-mentioned problems of the excessive current and of the graphite overheating. The duration of aluminothermic reduction is assumed to be 20 min, during which the reaction energy is released at the slag-metal interface. By studying the influence of the line voltage U_L on the modelling results, it was found that the line voltage below 40 V is acceptable for the furnace charge heating with three heating rods submerged into the melt. Figure 14 demonstrates the resulting evolution of the furnace temperature field.

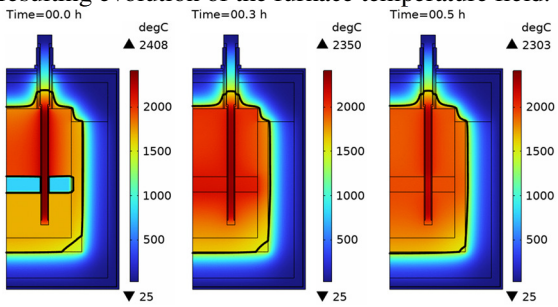

Figure 14. Temperature field evolution when both slag and metal are charged into the furnace. Line voltage is 40 V. Thick black line represents the slag melting temperature isoline (1540°C).

Computations show that the heating rod temperature reduces with time, as the electrical input power is below that provided during the preheating stage. The crucible temperature slowly increases with time due to the joint contribution of the electrical and chemical (≈ 890 kW) power input. If such transformer setting with $U_L = 40$ V was possible, it would result in approximately 180 kW of the

electrical power input, which would be enough to compensate heat losses and to maintain the charge above its melting point during a long period of time to maximise the chemical reaction output. In this hypothetical furnace configuration, the heating rod temperature stays below the maximum acceptable graphite temperature of 2500°C, and the effective line current I_L does not exceed the allowed maximum provided by the transformer.

6.4. Aluminothermic reduction with no external heating

The results of modelling the situation when no electrical power is provided are shown in Figure 15. In this case the maximum temperature in the furnace reduces faster with time than in the case with non-zero electrical power. Nevertheless, the aluminothermic reduction power alone is sufficient to maintain the melt in a liquid state during at least 30 minutes of the process.

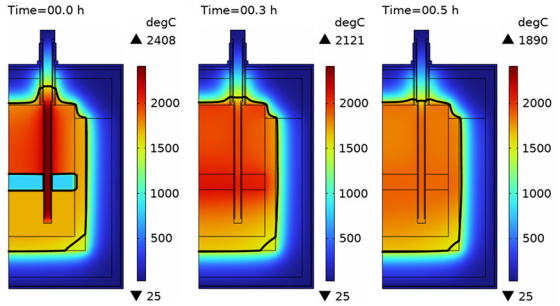

Figure 15. Temperature field evolution when both slag and metal are charged into the furnace with no electrical power input. Thick black line represents the slag melting temperature isoline (1540°C).

7. Conclusions

The present numerical model predicts that available electrical equipment is sufficient for preheating the empty ladle furnace up to 1600°C in less than 4 hours. Thanks to the model, the geometry of the heating rod was optimised to keep its temperature below 2500°C. It is found, however, that the electrical functioning of the furnace is strongly affected by the presence of the furnace charge, as both slag and metal are electrically conducting materials. The configuration where three heating rods are submerged into the molten charge is not acceptable, as it leads to the short-circuit between heating rods, to the effective line current I_L exceeding the allowed maximum provided by the transformer, and to the graphite overheating above the maximum acceptable temperature of 2500°C. The reduction of line voltage down to 40 V is found to be sufficient to avoid electrical and thermal damage of the furnace in configuration with heating rods submerged into the melt. Since this solution might be not possible, as it requires the replacement of existing transformer, a numerical study with no electrical power input has been performed. It shows that the aluminothermic reduction power alone is sufficient to maintain the melt in a liquid state during at least 30 minutes of the process. If an electrical insulation of heating rods from the melt could be found, it would result in a normal functioning of the electrical circuit even with the original transformer settings. However, in this case the overheating of graphite rods might be possible during the aluminothermic reduction process due to reaction heat. Thus, according to the model, switching off the electrical power supply is recommended for the duration of aluminothermic reduction process, when heating rods are submerged into the melt. The presented modelling approach for testing new furnace designs can be applied to other similar thermoelectrical problems.

References

[1] D. McEligot, W. D. Swank, D. L. Cottle and F. I. Valentin, "Thermal properties of G-348 graphite," *Idaho National Lab.(INL), Idaho Falls, ID (United States),* 2016.

[2] D. S. Smith, A. Alzina, J. Bourret, B. Nait-Ali, F. Pennec, N. Tessier-Doyen, K. Otsu, H. Matsubara, P. Elser and U. T. Gonzenbach, "Thermal conductivity of porous materials," *Journal of Materials Research,* vol. 28, no. 17, pp. 2260-2272, 2013.

[3] Entegris, Inc., *Properties and Characteristics of graphite, for the semiconductor industry.,* 2013.

[4] M. Leitner, T. Leitner, A. Schmon, K. Aziz and G. Pottlacher, "Thermophysical Properties of Liquid Aluminum," *METALLURGICAL AND MATERIALS TRANSACTIONS,* vol. 48, no. 6, p. 3036–3045, 2017.

[5] M. J. Assael, I. J. Armyra, J. Brillo, S. V. Stankus, J. Wu and W. A. Wakeham, "Reference data for the density and viscosity of liquid cadmium, cobalt, gallium, indium, mercury, silicon, thallium, and zinc," *J. Phys. Chem. Ref. Data,* vol. 41, no. 3, p. 033101, 2012.

[6] J. Bohdansky and H. E. J. Schins, "Surface tension and density of the liquid earth alkaline metals Mg, Ca, Sr, Ba," *Journal of Inorganic and Nuclear Chemistry,* vol. 30, no. 9, pp. 2331-2337, 1968.

[7] J. Xin, L. Gan, L. Jiao and C. Lai, "Accurate density calculation for molten slags in SiO2-Al2O3-CaO-MgO systems," *ISIJ International,* vol. 57, no. 8, pp. 1340-1349, 2017.

[8] K. Tang, S. Gouttebroze, X. Ma, Q. Du and C. van der Eijk, "Representation of the multiphysical properties of SiO2-Al2O3-CaO slags by deep neural networks," in *Proceedings of the 16th International Ferro-Alloys Congress (INFACON XVI)*, (virtual), 2021.

[9] K. Tang, C. van der Eijk, S. Gouttebroze, Q. Du, J. Safarian and G. Tranell, "Rheological properties of Al2O3--CaO--SiO2 slags," *Calphad,* vol. 77, p. 102421, 2022.

[10] A. T. Dinsdale and P. N. Quested, "The viscosity of aluminium and its alloys--A review of data and models," *Journal of materials science,* vol. 39, pp. 7221-7228, 2004.

[11] K. C. Mills, L. Yuan and R. T. Jones, "Estimating the physical properties of slags.," *J. S. Afr. Inst. Min. Metall.,* vol. 111, no. 10, pp. 649-658, 2011.

[12] COMSOL Documentation, "Sutherland's law," [Online]. Available: https://doc.comsol.com/5.5/doc/com.comsol.help.cfd/cfd_ug_fluidflow_high_mach.08.27.html.

[13] G. K. Burgess and P. D. Foote, "The emissivity of metals and oxides. IV. Iron oxide," *Journal of the Washington Academy of Sciences,* vol. 5, no. 11, pp. 377-378, 1915.

Acknowledgements

Authors acknowledge the financial support under the Horizon 2020 European Union project SisAl Pilot, Grant Agreement N°869268.